Geochemical Perspectives Letters

Molecular biosignatures in planetary analogue salts: implications for transport of organics in sulfate-rich brines beyond Earth

A. Moreras-Marti[1,2,#,*], M. Fox-Powell[3], J. Toney[2], A.C. McAdam[4], C. Slaymark[2], C.A. Knudson[4,5,6], J.M.T. Lewis[4,5,7], M.A. Salik[2], C.R. Cousins[1]

https://doi.org/10.7185/geochemlet.2434

Abstract

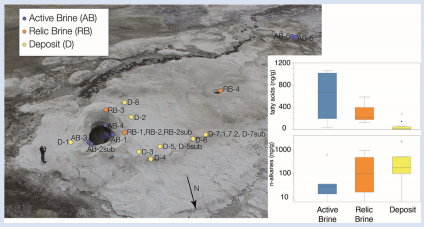

Salts formed during evaporation or freezing of brines can potentially incorporate organic matter that can inform about past biological activity. We analysed the lipid fraction preserved within the contemporary Lost Hammer salt deposit (Canadian High Arctic) - an analogue to extraterrestrial salt systems - and paired this with space mission-relevant evolved gas analysis. Our findings show microbial organic matter (fatty acids and *n*-alkanes) is incorporated into Lost Hammer salts, which comprise polyhydrated sulfates and chlorides. We find a difference in the relative abundance of fatty acids *vs.* *n*-alkanes indicating how these biosignatures evolve across active and non-active parts of the spring. We also find differences between pristine salt-organic mixtures and deposits that may have been remobilised by subsequent dissolution and recrystallisation. In this system, *n*-alkanes have the highest preservation potential, surviving the likely dissolution and recrystallisation of hydrated salt phases. This is important for considering the fate of organic matter on icy moons such as Europa, where salts emplaced on the surface by briny extrusions may have undergone fractional crystallisation, or where subsurface salts are remobilised by localised melting. It is also relevant for once active brine systems on Mars, where cycles of groundwater recharge and/or deliquescence led to dissolution and re-precipitation of evaporitic salts.

Received 15 March 2024 | Accepted 5 August 2024 | Published 10 September 2024

Introduction

Salt minerals precipitated during evaporation or freezing of brines can capture organic and geochemical biosignatures, preserving crucial information about the aqueous environment at the time of their formation (Schopf *et al.*, 2012). Such salts are prevalent throughout the Solar System, including Mars, icy moons, and asteroids. Their association with liquid water environments make salts high priority astrobiology targets (Phillips *et al.*, 2023). On Mars, sulfate salts are abundant globally and record major shifts in aqueous environment chemistry (Bibring *et al.*, 2006). Hydrated chloride and sulfate salts are suggested to be present on the surface of Europa (Brown and Hand, 2013), originating from a range of possible endogenous and/or exogenous processes, including emplacement from subsurface liquid reservoirs (King *et al.*, 2022). Chloride and carbonate salts sourced from subsurface water-rock reactions are components of ice grains in Enceladus plumes (Postberg *et al.*, 2009), and carbonate and chloride salts are present on dwarf planet Ceres, likely sourced from a liquid layer beneath the crust (De Sanctis *et al.*, 2020). Across all these targets, salt minerals have the potential to capture evidence of putative past or present microbial activity, in addition to abiogenic organic matter (Chan *et al.*, 2018).

Terrestrial environments containing hydrated and polyhydrated salts, similar to those found in extraterrestrial deposits can provide a framework for understanding the capture and detection of microbial organic biosignatures. Organic biosignatures, such as lipids, are fundamental components of cell structures and are utilised as molecular markers to identify microbial activity, environmental processes, and their stable carbon isotopic ratios can reveal autotrophic carbon fixation pathways (Jahnke *et al.*, 2019).

The analysis of materials from relevant planetary analogue environments with flight-like techniques can further support the interpretation of data from flight analyses of planetary materials. Evolved gas analysis mass spectrometry (EGA-MS) studies of salt-bearing planetary materials are currently being carried out by the Sample Analysis at Mars (SAM) instrument suite on the Mars Science Laboratory Curiosity rover (*e.g.*, Eigenbrode *et al.*, 2018). Similar thermal analyses are planned for future *in situ* planetary missions (Reinhardt *et al.*, 2020). The significance

1. School of Earth and Environmental Sciences, University of St Andrews, Irvine Building, North Street, Fife, UK, KY16 9AL
2. School of Geographical and Earth Sciences, Glasgow University, Molema Building, Glasgow, UK. G12 8QQ
3. AstrobiologyOU, The Open University, Milton Keynes, UK. MK7 6AA
4. NASA GSFC, Greenbelt, MD 20771
5. CRESST II, Greenbelt, MD 20771
6. University of Maryland, College Park, MD 20742
7. Department of Physics and Astronomy, Howard University, Washington, DC, USA
current address: School of Science, Auckland University of Technology, WS Building, Auckland, 1010, New Zealand
* Corresponding author (email: arola.moreras.marti@aut.ac.nz)

of this research lines in the combination of EGA-MS and molecular results, which have implications for past, current, and future *in situ* analyses on sulfate salts found throughout the Solar System.

Study Area

Axel Heiberg Island (Canadian High Arctic) hosts perennially cold hypersaline springs linked to sub-permafrost evaporite diapirs (Pollard *et al.*, 1999). The Lost Hammer (LH) spring (Fig. 1a) possesses the lowest temperature (–5 °C) and highest concentration of salt (24 %) of these springs, and releases gases dominated by methane (50 %) (Pollard *et al.*, 1999). During sampling of the LH spring in July 2017, the LH outflow brine originated from a single observable source comprising a salt dome with a ~2 m diameter central outlet (hereafter termed 'vent'; Fig. 1b). Adjacent to the vent dome, a ~1 m high salt apron extends ~100 m downslope, with a maximum width of ~50 m (hereafter termed 'apron deposit'; Fig. 1b). A dry cavity (~1 m diameter) in the apron deposit and associated dry channel indicated the likely location of past brine flow activity (hereafter referred to as 'relic brine'; Fig. 1b).

At time of sampling, the vent dome and apron deposit comprised sodium sulfates and chlorides of varying hydration states, with the highest abundances of sulfates closest to the vent (Fox-Powell *et al.*, 2019). Active microbial communities in LH vent and outflow stream are characterised by low concentrations of biomass in the sediments (around 10^5 cells/g) and lithotrophic microorganisms adapted to hypersaline and cold conditions: anaerobic methane oxidising archaea and sulfate reducing/sulfide oxidising bacteria are prevalent (Lay *et al.*, 2013; Lamarche-Gagnon *et al.*, 2015; Sapers *et al.*, 2017; Magnuson *et al.*, 2022). Quadruple Sulfur Isotope ($\delta^{34}S$, $\Delta^{33}S$ and $\Delta^{36}S$) analysis of iron sulfide from the outflow brine support these observations with fractionations typical of microbial sulfate reduction and sulfur disproportionation (Moreras-Marti *et al.*, 2021).

Methods

Between 15 to 40 g of salt were collected for each sample in polyethylene bags from the LH deposit and maintained at 4 °C as described in Fox-Powell *et al.* (2019). Samples were divided based on criteria of area: (1) Active Brine (AB) - within the active brine flow or source vent, (2) Relic Brine (RB) - samples on the outer edge of the vent and from the secondary dry vent and channel structure desribed above, but with no contact with actively liquid brine flow, and (3) Deposit (D) - older salt apron, with no contact with liquid brine channel. Samples D-7.1 and D-7.2 are two replicates from the same Deposit parent sample. Samples at depth ('sub') were collected at ~4 cm from the surface. Samples were freeze dried for organic biomarker extraction and analyses and EGA-MS; details are provided in Supplementary Information.

Results and Discussion

Sources of fatty acids and n-alkanes. Fatty acids (FA) exhibited a biological signature throughout the LH salt deposit (Fig. 2a,c). This was evidenced by the presence of short-to-mid chain FA (C_{12}-C_{24}) of even-over-odd preference, and C_{max} at C_{16} and C_{18}, the dominant FA lengths for bacteria and eukaryotic cells (López-Lara and Geiger, 2010). The greatest range in FA concentrations were observed in Active Brine salts (27.7 to 1072.5 ng/g; Fig. 2a), followed by Relic Brine salts (126.4 to 483.7 ng/g). The lowest concentration and range were observed in Deposit salts (6.9 to 277.3 ng/g). Several samples across the Active Brine and Relic Brine salts yielded branched FA (i- for iso-mer, a for anti-isomer). The i-C_{15}, a-C_{15}, i-C_{17} and a-C_{17} are interpreted to be associated with microbial sulfate reducers (MSR), while $C_{18:1}$ records the presence of cyanobacteria or other types of bacteria and algae (Perry *et al.*, 1979). Such branched FA have been identified in hypersaline lakes (Nichols *et al.*, 2023). Unsaturated i-C_{15} and a-C_{15} could not be identified as compounds under C_{16} had become degraded before measuring for branched and unsaturated FA. The presence of i-C_{17}, a-C_{17}

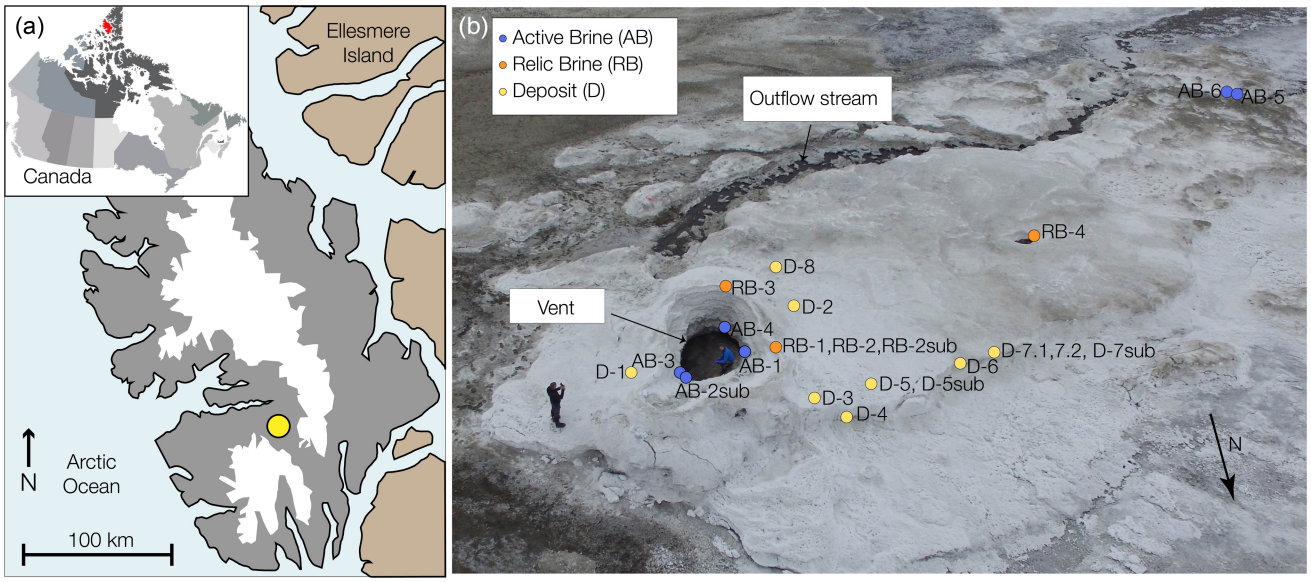

Figure 1 **(a)** Lost Hammer salt deposit location (yellow dot), Axel Heiberg Island. **(b)** Lost Hammer overview with geologist for scale. Sampling points are marked by coloured dots indicating the 3 different areas into which the Lost Hammer locality was divided: Active Brine, Relic Brine, and Deposit. Sample names ending in –sub indicate locations where a subsurface sample was paired with a corresponding surface salt.

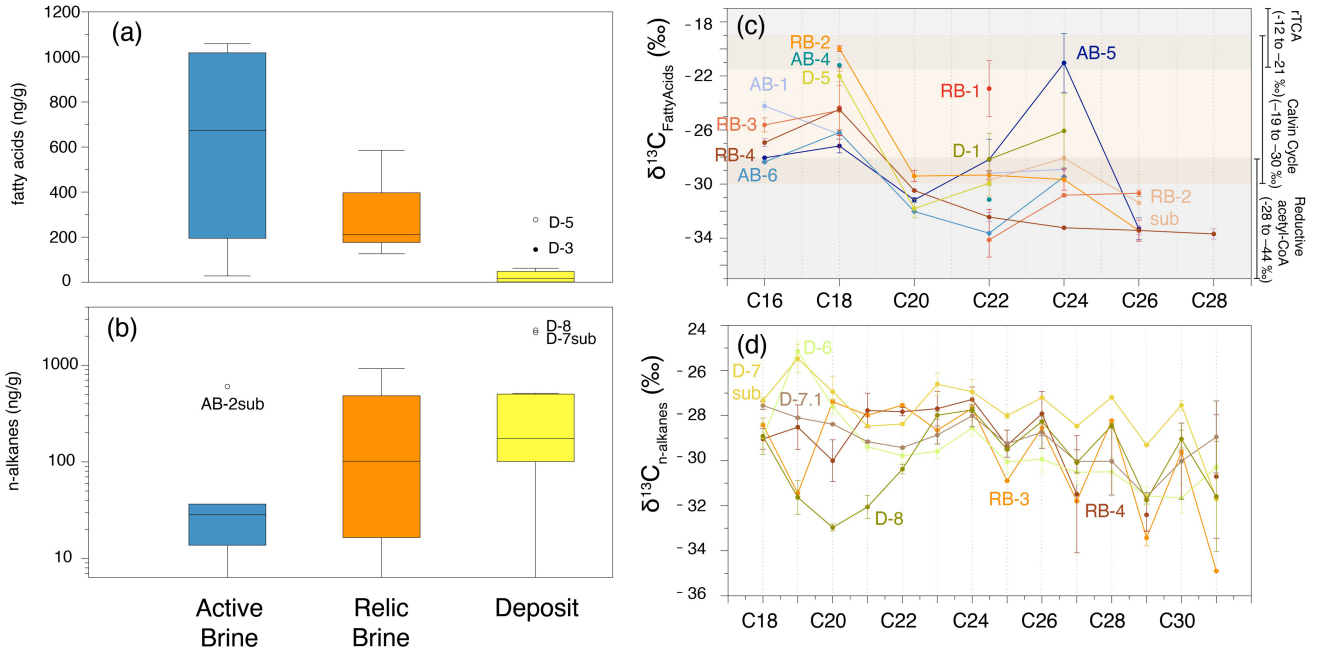

Figure 2 Whisker plot for **(a)** total FA and **(b)** total *n*-alkanes, concentrations in ng/g. The dots are outlier samples. Individual distributions can be found in Figures S-1, S-2 and S-3. Carbon isotopes from *n*-fatty acid compounds **(c)** and *n*-alkanes **(d).** The $\delta^{13}C$ values for FA range between –21 ± 2.17 ‰ to –34 ± 0.01 ‰. The $\delta^{13}C$ *n*-alkanes range between –25 ± 0.4 ‰ and –34 ± 0.01 ‰; complete data set in Table S-3.

and $C_{18:1}$ at the LH Deposit corroborates past studies of sulfur isotopes and microbial analyses which identified microbial sulfate reduction and sulfur oxidation occurring in the streams and vent sediments (Moreras-Marti *et al*, 2021; Magnuson *et al.*, 2022). Furthermore, the C isotope results from LH FA (C_{16} and C_{18} from –15 to –28 ‰ and >C_{20} from –21 to –34 ‰) (Fig. 2 c,d), fall in the ranges for autotrophic pathways with a mixed use of three assimilation pathways of carbon including: Reverse tricarboxylic acid (rTCA) cycle for autotrophic bacteria (from –12 to –21 ‰), Calvin cycle for cyanobacteria and algae (from –19 to –30 ‰) and reductive acetyl-CoA pathway for anaerobic bacteria and archaea (–28 to –44 ‰) (Jahnke *et al.*, 2019). The rapid degradation of FA through biological processes, occurring as quickly as a few weeks, underscores their presence in terrestrial environments as potential indicators of recent microbial activity (Perry *et al.*, 1979), such as observed in Active Brine samples, and to a lesser extent in Relic Brine samples. The limited occurrence of FA in Deposit samples is consistent with the absence of recent microbial activity and suggests rapid degradation of deposited compounds.

The *n*-alkanes and carbon isotope values indicate various biological sources in LH. The general prevalence of Medium Molecular Weight (MMW; C_{21} to C_{26}) over High Molecular Weight (HMW; >C_{27}) and Low Molecular Weight (LMW; <C_{20}) *n*-alkanes (Table 1) is indicative of algal and/or cyanobacteria sources (Castañeda and Shouten (2011), and references therein). The highest concentrations of *n*-alkanes (C_{16} to C_{32}) were observed in Deposit samples (13.7 to 2310.8 ng/g), followed by Relic Brine (16.48 to 923.4 ng/g) and lowest in Active Brine (34.6 to 603.5 ng/g) (Fig. 2b,c, Table 1). General odd/even dominance of HMW *n*-alkanes pointed to the contribution of higher plants and/or lichens which predominantely produce HMW *n*-alkanes (Castañeda and Shouten, 2011). Likewise samples RB-3, RB-4 and D-8 present *n*-alkane C_{max} peaks typical of higher plants as HMW *n*-alkanes are known to be major components of waxes in vascular land plants (Eglinton and Hamilton, 1967). No visible plant growth was observed within the outflow stream or LH salts themselves, so these are likely sourced from local tundra vegetation nearby LH or transported by aeolian processes. The LMW *n*-alkane distribution for all samples had no odd/even carbon number preference, suggesting derivation from microbial lipids, and/or microbial re-working of plant *n*-alkanes through early diagenesis (Castañeda and Shouten, 2011). The $\delta^{13}C$ of LMW *n*-alkanes varied between –27 and –32 ‰, the MMW –27 and –32 ‰ and HMW –28 and –34 ‰, suggesting an origin from bacteria, algae and or phytoplankton. The HMW *n*-alkanes $\delta^{13}C$ also suggested an input from C3 plants which usually exhibit a $\delta^{13}C$ of –34 to –35 ‰, (Castañeda and Shouten, 2011).

Association of molecular biosignatures with sulfate salts. A subset of seven representative samples capturing the full spatial distribution of the LH salt deposit were selected based on available remaining sample material for EGA-MS (Figs. 3, S-3). The EGA-MS results from Active Brine samples indicate CO_2, CH_4 or CH_3^- fragments of molecules evolving coincident with Na sulfate thermal decomposition at temperatures greater than 1000 °C (which results in SO_2 and O_2 evolution). These results suggest organic matter is associated with the sulfate phase of these mixed salt deposits, either contained within the salt crystal structure (*e.g.*, in fluid inclusions) or hosted on crystal surfaces/along crystal boundaries and are partially oxidised by co-evolved O_2 to CO_2. If associated with the salt, we propose some organic biosignatures (including FA and *n*-alkanes) may have been captured from the brine when salts precipitated. These biosignatures may have either nucleated or co-precipitated with the salts, becoming associated with or encapsulated within primary salt crystals, thereby protecting them against oxidation mechanisms (Keil and Mayer, 2014). The CO_2 evolution in some samples could be attributed to minor carbonates, observed by LH by Battler *et al.* (2013). In RB-3, D-5 and D-7sub (Fig. 3b), the first CO_2 peak around 650 °C could result from thermal decomposition of a Mg-bearing carbonate, and a second sharp CO_2 peak around 785 °C could indicate Ca carbonate. However, in these samples there is likely organic oxidation indicated by a peak at ~500 °C in EGA-MS traces for CO_2, alkane fragments and CH_4/ CH_4 fragments.

Table 1 Organic biomarker results for FA and *n*-alkanes. Total Lipid Extract (TLE). Average Chain Length (ACL) for *n*-fatty acids and *n*-alkanes calculated following equations from Carrizo *et al.* (2019). FA (branched and non-branched) and *n*-alkane concentrations are split into concentrations of Low Molecular Weight (LMW) and High Molecular Weight (HMW) compounds. Non-detected as 'nd', equations with non-detected carbon chains as '-', below detection as "BD".Complete data set in Table S-1 and S-2 for FA and for *n*-alkanes.

Sample ID	TLE (mg/g)	Fatty acids (FA) (ng/g)	ACL (C_{14}-C_{26})	LMW (C_{14}-C_{20}) (ng/g)	HMW (C_{20}-C_{26}) (ng/g)	*n*-alkanes (ng/g)	ACL (C_{16}-C_{31})	LMW (C_{16}-C_{20}) (ng/g)	HMW (C_{27}-C_{31}) (ng/g)
Active Brine									
AB-1	0.09	1018.1	17	926.0	92.1	22.1	23	3.9	0
AB-2sub	4.86	588.5	17	559.6	30.0	603.5	24	83.5	177.2
AB-3	0.58	27.7	19	15.0	12.8	34.6	23	7.6	6.2
AB-4	0.75	194.7	17	193.8	6.4	36.6	23	6.6	6.8
AB-5	0.06	758.1	18	636.8	142.0	Nd	-	-	-
AB-6	0.05	1058.9	17	923.8	148.7	13.7	24	-	2.7
Relic Brine									
RB-1	0.09	210.8	18	145.0	65.8	101.5	23	28.4	21.5
RB-2	0.03	176.5	18	161.3	20.4	16.5	21	7.2	-
RB-2sub	0.07	396.9	19	280.8	116.0	nd	-	-	-
RB-3	0.18	126.4	18	107.5	18.9	923.4	24	195.6	326.9
RB-4	0.48	585.3	18	503.6	81.7	483.8	24	115.8	104.6
Deposit									
D-1	0.23	33.7	18	28.7	5.0	25.1	23	4.3	1.8
D-2	0.22	62.1	17	62.1	BD	128.4	24	21.5	32.2
D-3	0.04	145.1	18	129.5	16.6	84.7	24	8.03	18.97
D-4	0.07	nd	-	-	-	nd	-	-	-
D-5	0.05	277.3	17	273.2	11.9	117.2	22	37.5	16.7
D-5sub	0.05	22.2	17	22.2	0.0	193.1	23	51.4	45.4
D-6	0.08	2.4	22	0.0	2.4	512.8	23	134.8	106.7
D-7.1	0.10	16.4	19	11.5	4.9	494.3	23	151.4	100.6
D-7.2	0.10	6.1	16	6.1	0.0	174.8	24	26.3	48
D-7sub	0.25	nd	-	-	-	2181.3	23	749.1	413.1
D-8	0.90	6.9	-	6.9	-	2310.8	23	657.4	555.4

Post-depositional recrystallisation of salts at LH may account for differences in organic profiles and EGA-MS traces observed between samples. For example, dissolution and recrystallisation can release organic compounds from close association with salt crystals at lower temperatures. The lower temperature (~500 °C) evolution of CO_2 from D-7sub (Fig. 3e), not seen in Active Brine samples, likely reflects oxidation of organics not captured within salts, which could have been released by dissolution. EGA-MS results show a single defined SO_2 peak for Active Brine (Fig. 3a) samples but these peaks decrease in sharpness and definition for Relic Brine and Deposit samples (*e.g.*, RB-3, D-7; Fig. 3b,d). Relic Brine/Deposit samples exhibit additional SO_2 peaks, as exemplified by D-7sub where multiple weakly defined peaks evolve across a range of temperatures. Multiple evolutions of SO_2 are suggestive of multiple sulfate phases present, which could have formed in Deposit samples as a consequence of multiple cycles of dissolution and recrystallisation in these metastable salts. Specifically, the temperatures of SO_2 evolution suggest some Mg-bearing sulfates in addition to Na sulfates. Furthermore, the likely presence of carbonates in samples RB-3, D-5sub and D-7sub, which were not observed in Active Brine samples, would suggest re-working and alteration of Relic Brine and Deposit samples.

If FA are among the compounds initially trapped by salt crystallisation in Active Brine locations, such re-working would liberate them, enabling degradation and lower FA abundances observed in Relic Brine and Deposit samples. Mirabilite and thenardite, sodium sulfate minerals detected in LH salts (Fox-Powell *et al.*, 2019), are sensitive to atmospheric humidity and can transition readily between hydration states. Dynamic changes to the hydration state of salt deposits over short (daily to seasonal) time scales have been observed at the LH salt deposit (Battler *et al.*, 2013; this fieldwork). The organic molecules found to survive the re-working process in the Deposit salts, distal to the active brine flow in LH salts, are *n*-alkanes.

Implications for Detection of Organic Biosignatures in Planetary Salts

We have identified associations between microbial organic biosignatures and sulfate salts in a system relevant to past and present extraterrestrial brine environments. The relative abundance of FA *versus* n-alkanes reveals lipids evolving across active and non-active parts of the LH salt deposit. We show differences between lipids incorporated directly into precipitating salts and those remobilised by subsequent salt dissolution and recrystallisation. Our findings suggest that n-alkanes are more resilient, surviving dissolution and recrystallisation, and are found in deposits distal from active brine flow. These results have implications for the transport and preservation of organic biosignatures in low temperature planetary salts.

Encapsulated lipids in salts can record evidence of specific metabolic activities, such as microbial sulfate reduction (MSR) and autotrophic pathways, through their isotopic and molecular signatures. Additionally, coeval salt precipitation and organic

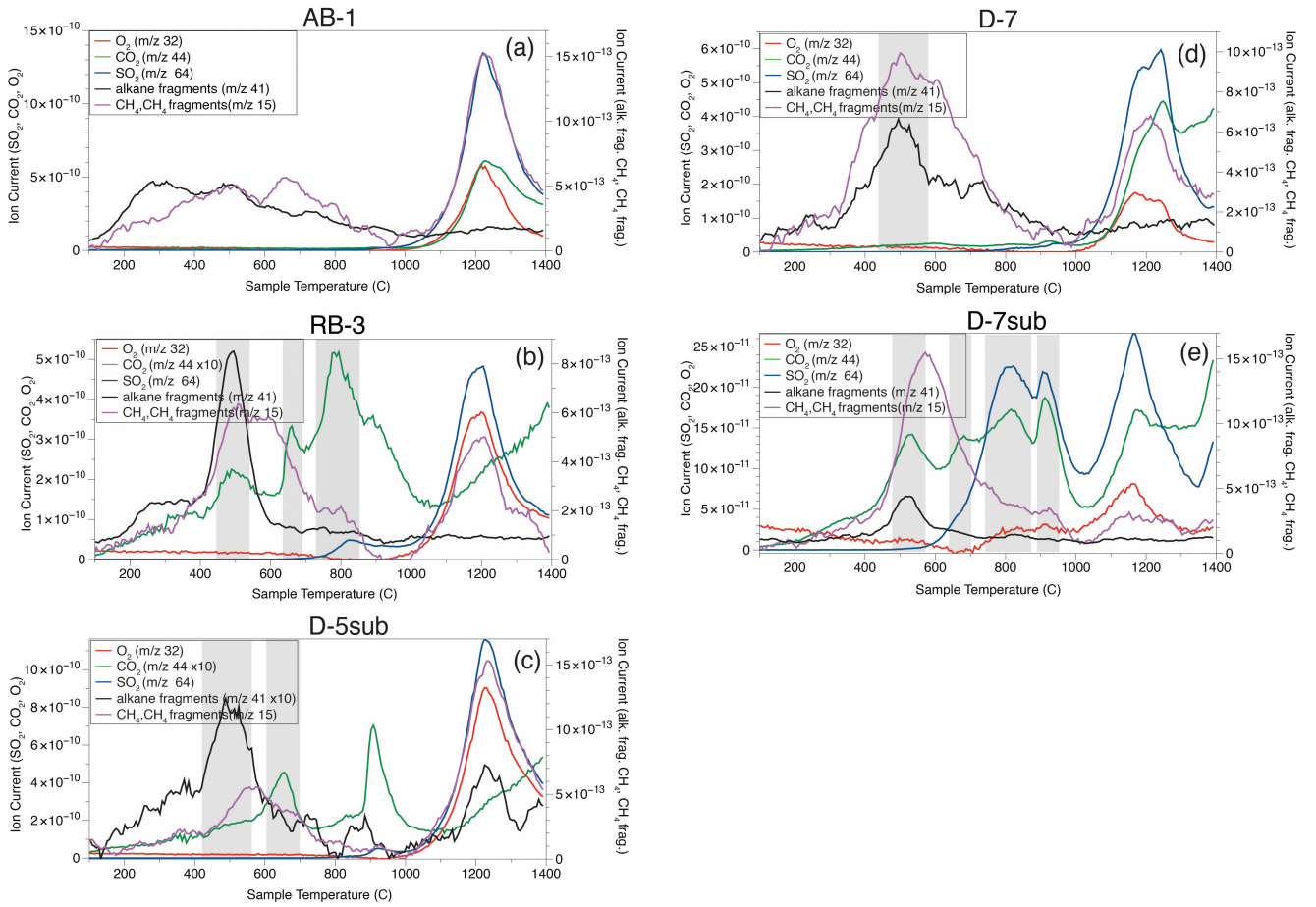

Figure 3 Subset representing measured samples for EGA-MS, complete sample set in Figure S-4. **(a)** Active Brine sample AB-1, **(b)** Relic Brine sample RB-3, **(c)** Deposit sample D-5sub, **(d)** D-7.1 and **(e)** D-7sub. All samples evolve SO_2 (m/z 64), O_2 (m/z 32), and CO_2 (m/z 44) during heating at temperatures up to 1400 °C. All samples apart from RB-3 show the evolution of likely alkane fragments (*e.g.*, signal at m/z 41) and possible methane (either discrete methane or CH_3 fragments of a larger organic molecule; signal at m/z 15; see SI). Grey area indicates peaks of interest discussed in text.

capture offer insight into environmental conditions and geochemistry at the time of formation.

EGA-MS results indicate that organics are associated with sulfate salt minerals and likely co-precipitate in Active Brine samples. Salts can protect organic molecules from degradation *via* UV radiation and oxidising agents (Keil and Mayer, 2014). EGA-MS can also detect secondary changes in salt mineralogy, such as re-precipitation with different cations or hydration states. These changes are identified by EGA-MS through variations in thermal decomposition or thermal dehydration temperatures, as seen with Mg and Na sulfates.

Studies on lipid biomarkers from hypersaline Mars analogues have also found organics preserved in sulfate salts, even in extreme acidic conditions like the Dallol hydrothermal system (Carrizo *et al.*, 2019; Nichols *et al.*, 2023). A hypersaline lake study using spectroscopy showed mirabilite ($NaSO_4$) hosting organic molecules (Gill *et al.*, 2023). A common factor in all studies is that extreme conditions (temperature, pH, salinity) serve as strategies for lipid biomarker preservation (Finkel *et al.*, 2023).

In salt deposits resulting from upwelling of subsurface brines, the transport, alteration, and distribution of molecular biosignatures will be influenced by salt crystallisation dynamics. The encapsulation of lipids within sulfate minerals implies that lipids should be most prevalent where sulfate minerals first precipitate. However, if subsequent dissolution and recrystallisation release molecules from salt crystals, there is an opportunity for post-depositional liquid-phase degradation or further transport away from the original deposition site. This is particularly important for predicting organic transport on icy worlds such as Europa, where cryovolcanic salts may have undergone fractional crystallisation or partial remobilisation of crystallised brine in the subsurface (Steinbrügge *et al.*, 2020). Similarly, on Mars, where cycles of groundwater recharge and/or deliquescence led to dissolution and re-precipitation of evaporitic salts (Abotalib and Heggy, 2019), this could remobilise primary phase organic matter.

Future missions should focus on collecting (i) samples near upwelling brines; given that FA are more prevalent where Na sulfate minerals first precipitate, (ii) salts with multiple dissolution and recrystallisation phases; to reveal long term preservation mechanisms on planetary salt deposits. Key measurements to identifying these processes will be EGA-MS, isotopic, and molecular analysis.

Acknowledgements

This work was funded by Leverhulme Research Project Grant RPG-2019-353. We also thank Gordon Osinski and the Polar Continental Shelf Program (Natural Resources Canada) for logistical field support.

Editor: Francis McCubbin

Additional Information

Supplementary Information accompanies this letter at https://www.geochemicalperspectivesletters.org/article2434.

Cite this letter as: Moreras-Marti, A., Fox-Powell, M., Toney, J., McAdam, A.C., Slaymark, C., Knudson, C.A., Lewis, J.M.T., Salik, M.A., Cousins, C.R. (2024) Molecular biosignatures in planetary analogue salts: implications for transport of organics in sulfate-rich brines beyond Earth. *Geochem. Persp. Let.* 32, 1–6. https://doi.org/10.7185/geochemlet.2434

References

Abotalib, A.Z., Heggy, E. (2019) A deep groundwater origin for recurring slope lineae on Mars. *Nature Geoscience* 12, 235–241. https://doi.org/10.1038/s41561-019-0327-5

Battler, M.M., Osinski, G.R., Banerjee, N.R. (2013) Mineralogy of saline perennial cold springs on Axel Heiberg Island, Nunavut, Canada and implications for spring deposits on Mars. *Icarus* 224, 364–381. https://doi.org/10.1016/j.icarus.2012.08.031

Bibring, J.P., Langevin, Y., Mustard, J.F., Poulet, F., Arvidson, R., *et al.* (2006) Global mineralogical and aqueous Mars history derived from OMEGA/Mars Express data. *Science 312,* 400–404. https://doi.org/10.1126/science.1122659

Brown, M.E., Hand, K.P. (2013) Salts and radiation products on the surface of Europa. *The Astronomical Journal* 145, 110. https://doi.org/10.1088/0004-6256/145/4/110

Carrizo, D., Sánchez-García, L., Rodriguez, N., Gómez, F. (2019) Lipid biomarker and carbon stable isotope survey on the Dallol hydrothermal system in Ethiopia. *Astrobiology* 19, 1474–1489. https://doi.org/10.1089/ast.2018.1963

Castañeda, I.S., Schouten, S. (2011) A review of molecular organic proxies for examining modern and ancient lacustrine environments. *Quaternary Science Reviews* 30, 2851–2891. https://doi.org/10.1016/j.quascirev.2011.07.009.

Chan, Q.H., Zolensky, M.E., Kebukawa, Y., Fries, M., Ito, M., *et al.* (2018) Organic matter in extraterrestrial water-bearing salt crystals. *Science Advances* 4, eaao3521. https://doi.org/10.1126/sciadv.aao3521

De Sanctis, M.C., Ammannito, E., Raponi, A., Frigeri, A., Ferrari, M., *et al.* (2020) Fresh emplacement of hydrated sodium chloride on Ceres from ascending salty fluids. *Nature Astronomy* 4, 786–793. https://doi.org/10.1038/s41550-020-1138-8

Eglinton, G., Hamilton, R.J. (1967) Leaf Epicuticular Waxes: The waxy outer surfaces of most plants display a wide diversity of fine structure and chemical constituents. *Science* 156, 1322–1335. https://doi.org/10.wa1126/science.156.3780.1322

Eigenbrode, J.L., Summons, R.E., Steele, A., Freissinet, C., Millan, M., *et al.* (2018) Organic matter preserved in 3-billion-year-old mudstones at Gale crater, Mars. *Science* 360, 1096–1101. https://doi.org/10.1126/science.aas9185

Finkel, P.L., Carrizo, D., Parro, V., Sánchez-García, L. (2023) An Overview of Lipid Biomarkers in Terrestrial Extreme Environments with Relevance for Mars Exploration. *Astrobiology* 23, 563–604. https://doi.org/10.1089/ast.2022.0083

Fox-Powell, M.G., Osinski, G.R., Applin, D., Stromberg, J.M., Gázquez, F., *et al.* (2019) Natural analogue constraints on Europa's non-ice surface material. *Geophysical Research Letters* 46, 5759–5767. https://doi.org/10.1029/2018GL081339

Gill, K.K., Jagniecki, E., Benison, K.C., Gibson, M.E. (2023) A Mars-analog sulfate mineral, mirabilite, preserves biosignatures. *Geology* 51, 818–822. https://doi.org/10.1130/G51256.1

Jahnke, L.L., Des Marais, D.J. (2019) Carbon isotopic composition of lipid biomarkers from an endoevaporitic gypsum crust microbial mat reveals cycling of mineralized organic carbon. *Geobiology* 17, 643–659. https://doi.org/10.1111/gbi.12355

Keil, R.G., Mayer, L.M. (2014) Mineral matrices and organic matter. *Treatise on Geochemistry* 337–359. https://doi.org/10.1016/B978-0-08-095975-7.01024-X

King, O., Fletcher, L.N., Ligier, N. (2022) Compositional mapping of Europa using MCMC modeling of near-IR VLT/SPHERE and Galileo/NIMS observations. *The Planetary Science Journal* 3, 72. https://doi.org/10.3847/PSJ/ac596d

Lay, C.Y., Mykytczuk, N.C., Yergeau, E., Lamarche-Gagnon, G., Greer, C.W., Whyte, L.G. (2013) Defining the functional potential and active community members of a sediment microbial community in a high-arctic hypersaline subzero spring. *Applied and Environmental Microbiology* 79, 3637–3648. https://doi.org/10.1128/AEM.00153-13

Lamarche-Gagnon, G., Comery, R., Greer, C.W., Whyte, L.G. (2015) Evidence of in situ microbial activity and sulphidogenesis in perennially sub-0°C and hypersaline sediments of a high Arctic permafrost spring. *Extremophiles* 19, 1–15. https://doi.org/10.1007/s00792-014-0703-4

López-Lara, I.M., Geiger, O. (2010) Formation of fatty acids. In: Timmis, K.N. (Ed.) *Handbook of Hydrocarbon and Lipid Microbiology*. Springer, Berlin, Heidelberg. https://doi.org/10.1007/978-3-540-77587-4_26

Magnuson, E., Altshuler, I., Fernández-Martínez, M.Á., Chen, Y.J., Maggiori, C., *et al.* (2022) Active lithoautotrophic and methane-oxidizing microbial community in an anoxic, sub-zero, and hypersaline High Arctic spring. *The ISME Journal* 16, 1798–1808. https://doi.org/10.1038/s41396-022-01233-8

Moreras-Marti, A., Fox-Powell, M., Stueeken, E., Di Rocco, T., Galloway, T., *et al.* (2021) Quadruple sulfur isotope biosignatures from terrestrial Mars analogue systems. *Geochimica et Cosmochimica Acta* 308, 157–172. https://doi.org/10.1016/j.gca.2021.06.007

Nichols, F., Pontefract, A., Dion-Kirschner, H., Masterson, A.L., Osburn, M.R. (2023) Lipid Biosignatures From SO4-Rich Hypersaline Lakes of the Cariboo Plateau. *Journal of Geophysical Research: Biogeosciences* 128, e2023JG007480 https://doi.org/10.1029/2023JG007480

Perry, G.J., Volkman, J.K., Johns, R.B. (1979) Fatty Acids of Bacterial Origin in Contemporary Marine Sediments. *Geochimica et Cosmochimica Acta* 43, 1715–1725. https://doi.org/10.1016/0016-7037(79)90020-6

Phillips, M.S., McInenly, M., Hofmann, M.H., Hinman, N.W., Warren-Rhodes, K., *et al.* (2023). Salt Constructs in Paleo-Lake Basins as High-Priority Astrobiology *Targets. Remote Sensing* 15, 314. https://doi.org/10.3390/rs15020314

Pollard, W., Omelon, C., Andersen, D., McKay, C. (1999) Perennial spring occurrence in the Expedition Fiord area of western Axel Heiberg Island, Canadian high Arctic. *Canadian Journal of Earth Sciences* 36, 105–120. https://doi.org/10.1139/e98-097

Postberg, F., Kempf, S., Schmidt, J., Brilliantov, N., Beinsen, A., *et al.* (2009) Sodium salts in E-ring ice grains from an ocean below the surface of Enceladus. *Nature* 459, 1098–1101. https://doi.org/10.1038/nature08046

Reinhardt, M., Goetz, W., Thiel, V. (2020) Testing flight-like pyrolysis gas chromatography–mass spectrometry as performed by the Mars Organic Molecule Analyzer onboard the ExoMars 2020 rover on Oxia Planum analog samples. *Astrobiology* 20, 415–428. https://doi.org/10.1089/ast.2019.2143

Sapers, H.M., Ronholm, J., Raymond-Bouchard, I., Comrey, R., Osinski, G.R., Whyte, L.G. (2017) Biological characterization of microenvironments in a hypersaline cold spring Mars analog. *Frontiers in Microbiology* 8, 2527.https://doi.org/10.3389/fmicb.2017.02527

Schopf, J.W., Farmer, J.D., Foster, I.S., Kudryavtsev, A.B., Gallardo, V.A., Espinoza, C. (2012) Gypsum-permineralized microfossils and their relevance to the search for life on Mars. *Astrobiology* 12, 619–633. https://doi.org/10.1089/ast.2012.0827

Steinbrügge, G., Voigt, J.R., Wolfenbarger, N.S., Hamilton, C.W., Soderlund, K.M., *et al.* (2020) Brine migration and impact-induced cryovolcanism on Europa. *Geophysical Research Letters* 47, e2020GL090797. https://doi.org/10.1029/2020GL090797

Geochemical Perspectives Letters

Molecular biosignatures in planetary analogue salts: implications for transport of organics in sulfate-rich brines beyond Earth

A. Moreras-Marti, M. Fox-Powell, J. Toney, A.C. McAdam, C. Slaymark, C.A. Knudson, J.M.T. Lewis, M.A. Salik, C.R. Cousins

Supplementary Information

The Supplementary Information includes:

- Methodology
- Figures S-1 to S-4
- Supplementary Tables S-1 to S-3
- Supplementary Information References

Methodology

1. Lipid analysis

Molecular biosignatures were extracted at the BECS organic geochemistry lab at the University of Glasgow, Glasgow, UK, following the BECS lipid biomarker extraction protocol (Toney *et al.,* 2010) with freeze-dried salt sample material, not powdered. Due to the low concentration of organic matter in the salts, between 3.8 and 22.7 g of sample were used. All glass vials used for this procedure were combusted at 450 °C for 8 hr prior to analysis. The total lipid extract (TLE) was separated from salt matrices using a Dionex Accelerated Solvent Extractor (ASE) 350 with a mixture of dichloromethane and methanol (9:1 DCM;MeOH). Solvent was evaporated from the TLE using nitrogen in a Turbovap and the weight of TLE was recorded. The TLE was then separated into neutral and acid fractions using solid phase extraction (SPE). SPE was performed using silica columns comprised of a glass wool stopper in a Pasteur pipette with, ~4cm dry aminopropyl silica gel, topped with combusted sand. Columns were washed with 3 bed volumes of 1:1 DCM_isopropyl alcohol (ISO) before the TLE was loaded onto the column using 1:1 DCM:ISO solution. Subsequently the Total Neutral Fraction (TNF) was eluted with 4 mL1:1 DCM:ISO and collected into an 8 mL vial. Following, the Total Acid Fraction (TAF) was eluted with 4 mLof ether with 4% acetic acid, and TAF collected in an 8 mL vial. The TNF was further separated using a second silica SPE column. TNF was separated on 35-70 µm particle size silica powder. Columns were washed with 3 bed volume of hexane before TNF was loaded on to the column. Columns were

eluted with hexane to obtain the non-polar, aliphatic hydrocarbon fraction containing *n*-alkanes. Branched fatty acids I-15 and a-15 were not observed as anything lower than C16 had evaporated by the time the branched fatty acid analysis was performed.

n-Alkanes were analysed on an Agilent 7890B gas chromatography flame ionisation detector (GC-FID). The GC-FID was fitted with an Agilent Rtx-1 column (60 m length, 250 µm i.d., 0.25 µm film thickness). Hydrogen was used as the carrier gas at a 1.2ml/min constant flow rate. The method used splitless injection (1µl) and the oven temperature was programmed from 60 °C (held for 2 mins) to 120 °C at a rate of 30 °C/min, then ramped to 330 °C at a rate of 5 °C/min and held for 15 minutes. An external standard mix of C_{16}, C_{18}, C_{19}, C_{23}, C_{25}, C_{26}, C_{28}, C_{30}, C_{32}, C_{37} was measured every 10 samples and used to identify retention times of *n*-alkanes in sediment samples. The *n*-alkanes were quantified using an external calibration of the standard mix ranging from 2.5- 10 µg/ml. Each chain length identified in samples was calibrated to its chain length in the standard mix or if not present in the standard mix, the closest chain length was chosen (e.g., C_{27} calibrated using C_{28} in the standard mix).

A sample of derivatized fatty acids (as FAMEs) were run on an Agilent 7890B Series GC with 5977A GC-EI mass spectrometer with helium as a carrier gas and GC method was the same as the GC-FID outlined above. Fatty acid presence was confirmed using the ion chromatograms of the corresponding homologue's fatty acid methyl ester (FAME) ion chromatogram. Straight chain and branched FAMEs are characterised by the presence of m/z 74 and 84. Unsaturated FAMEs had similar ion chromatograms but with a suppressed m/z 74. Identity of compounds was also confirmed by comparison to known ion chromatograms reported in Sanchez Garcia *et al.*, (2018).

Stable carbon isotopes were analysed for samples presenting enough concentration of *n*-fatty acids (AB-1, AB-4, AB-5, AB-6, RB-1, RB-2, RB-2sub, RB-3, RB-4, D-1, D-5) and *n*-alkanes (RB-3, RB4, D-6, D-7.1, D-7sub, D-8). The samples were analysed on an Agilent 7890B GC-FID connected to an Isoprime 100 Mass Spectrometer (Elementar). The GC-FID was fitted with an Agilent Rtx-1 column (60 m length, 250 µm internal diameter, 0.25 µm film thickness). Hydrogen was used as the carrier gas at a 1.2ml/min constant flow rate. The GC method used splitless injection (1µl) and the oven temperature was programmed from 60 °C (held for 2 mins) to 120 °C at a rate of 30 °C/min, then ramped to 325 °C at a rate of 5 °C/min and held for 16 minutes. Samples were measured in duplicate and $\delta^{13}C$ values were converted to the V-PBD scale by linear regression to an in-house standard of known $\delta^{13}C$. Standards were measured in duplicate every 10 samples and in triplicate at the start and end of each batch. The in-house standard was characterised using Indiana B5 containing C_{16} to C_{30} alkanes with an isotopic range between –26.15 and –40.9 ‰. Instrument precision on duplicate analysis of standards gave a standard deviation of <1. Samples that gave higher than 3‰ excluded from

results as concentrations were not high enough to obtain reasonable precision. The mean and 1 standard deviation are reported in results.

1. Evolved Gas Analysis (EGA)

Evolved Gas Analysis (EGA) was conducted to constrain sample mineralogy and investigate potential associations between organic compounds and salt phases. EGA-MS was carried out with a Setaram LabSys-Evo Thermo-gravimeter/Differential Scanning Calorimeter interfaced to a Pfieffer OmniStar quadrupole mass spectrometer. Five milligrams of freeze-dried sample was loaded into the EGA-MS pyrolysis oven and heated from 70 to 1400 °C, with a ramp rate of 35 °C/minute. A He carrier gas was used at a flow rate of 5 mL/min, and a pressure of ~25 millibar was maintained inside the oven during the pyrolysis run. Any gases evolved during heating were carried to the MS where they were identified by the mass-to-charge ratio (m/z) of the molecule or one of its MS fragments. Here we focused on SO_2 (m/z 64), CO_2 (m/z 44), O_2 (m/z 32), alkane fragments (e.g., m/z 39, 41) and m/z 15 which may result from methane or CH3 fragments of a larger organic molecule (studied using the signal at m/z 15; m/z 16 was not used directly because of several mass interferences at m/z 16 (e.g., O MS fragments of SO_2 and CO_2) but less mass interferences occur at the m/z 15 MS fragment of methane (CH_3^-)) or CH3 fragments of a larger organic molecule).

Supplementary Figures

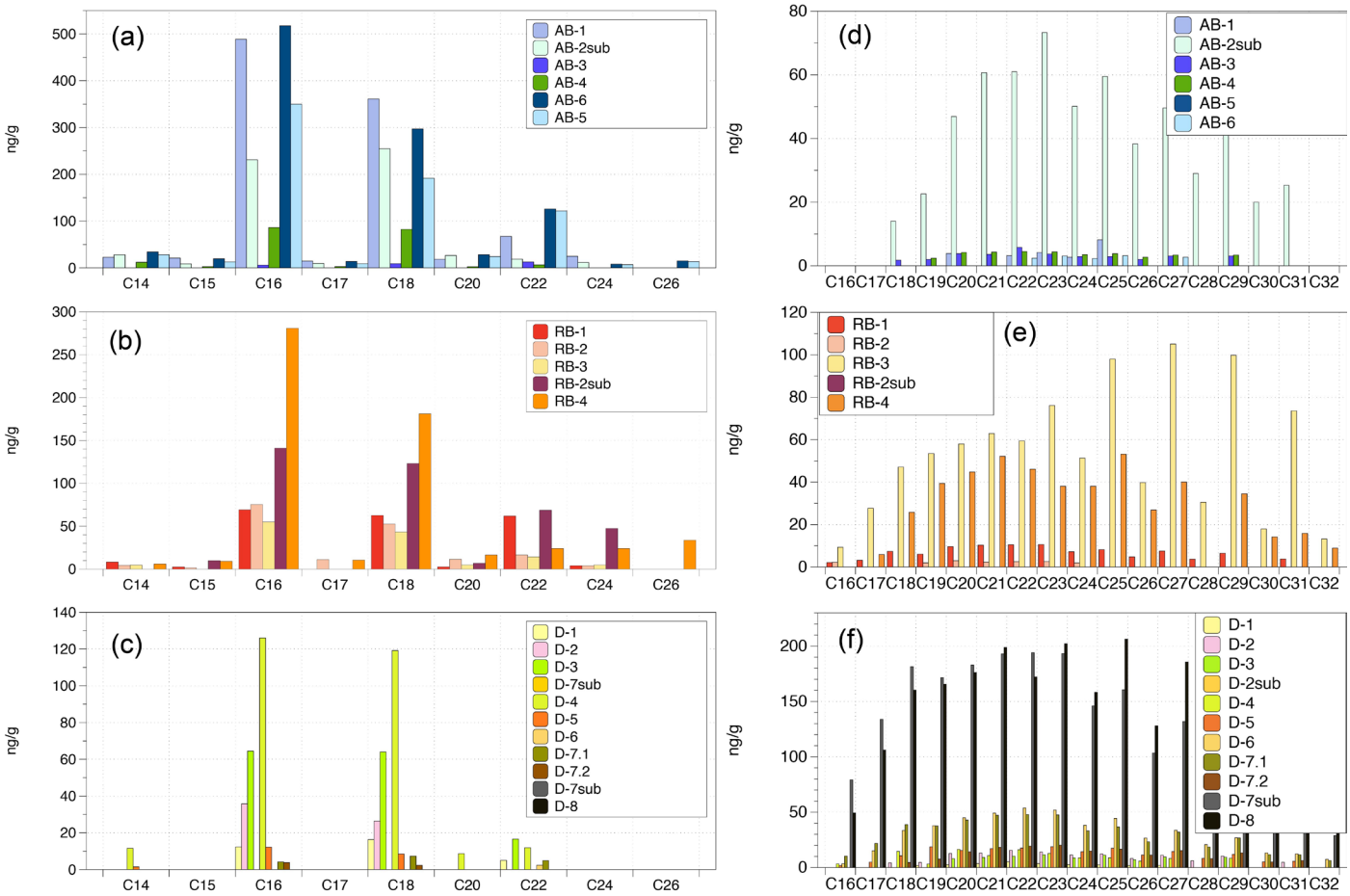

Figure S-1 (a-c) FAMES distribution for **(a)** Active Brine samples, **(b)** Relic Brine samples, and **(c)** Deposit samples. **(d-f)** Distribution of n-alkanes for **(d)** Active Brine samples, **(e)** Relic Brine samples, and **(f)** Deposit samples.

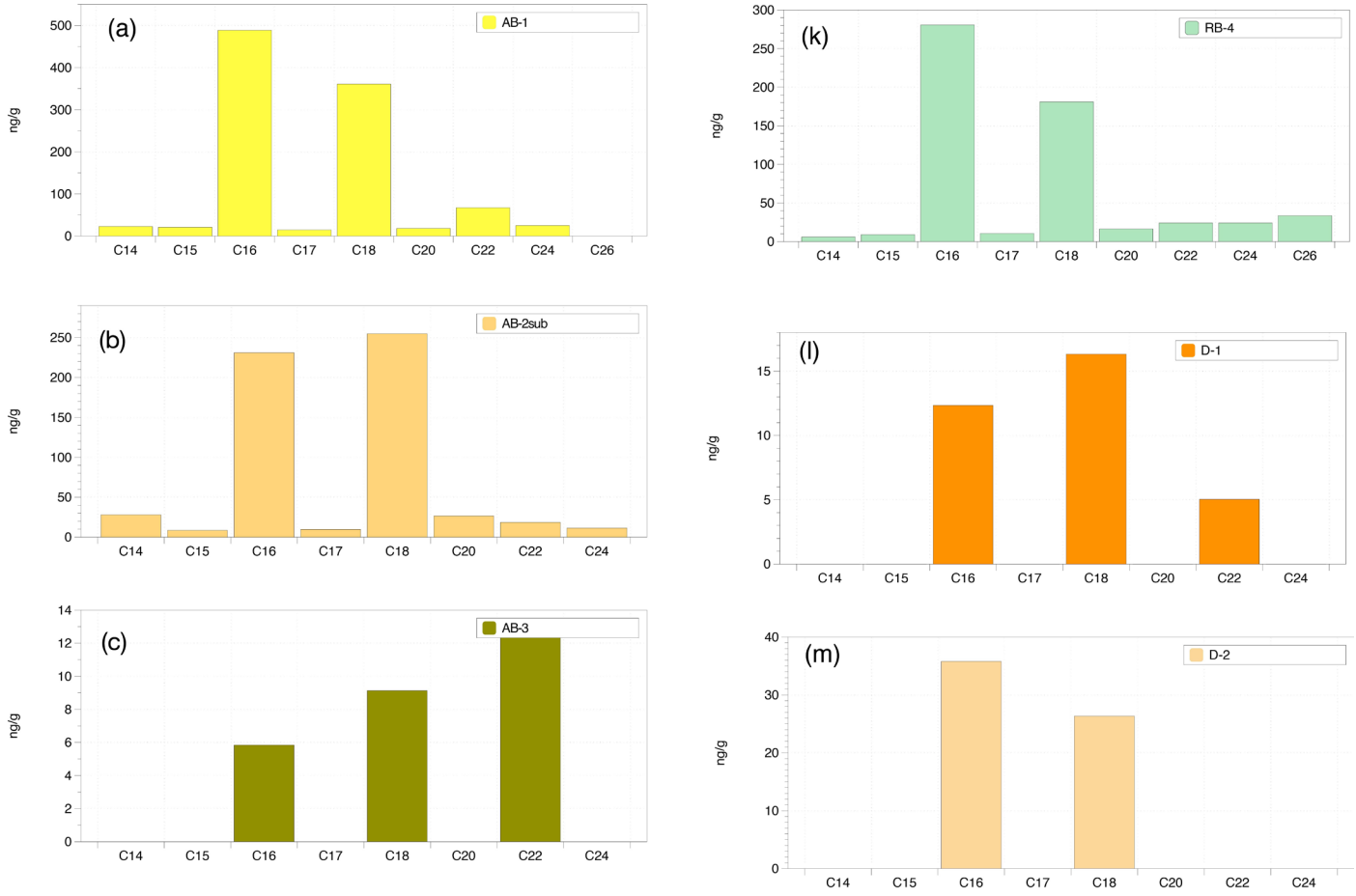

Figure S-2 (across 3 pages) Individual fatty acid distribution for all different samples. Samples D-4 and D-7sub didn't present any alkanes. On the other hand, D-8 presented only C18:1 unsaturated, which are not counted for these graphs.

Figure S-2 continued

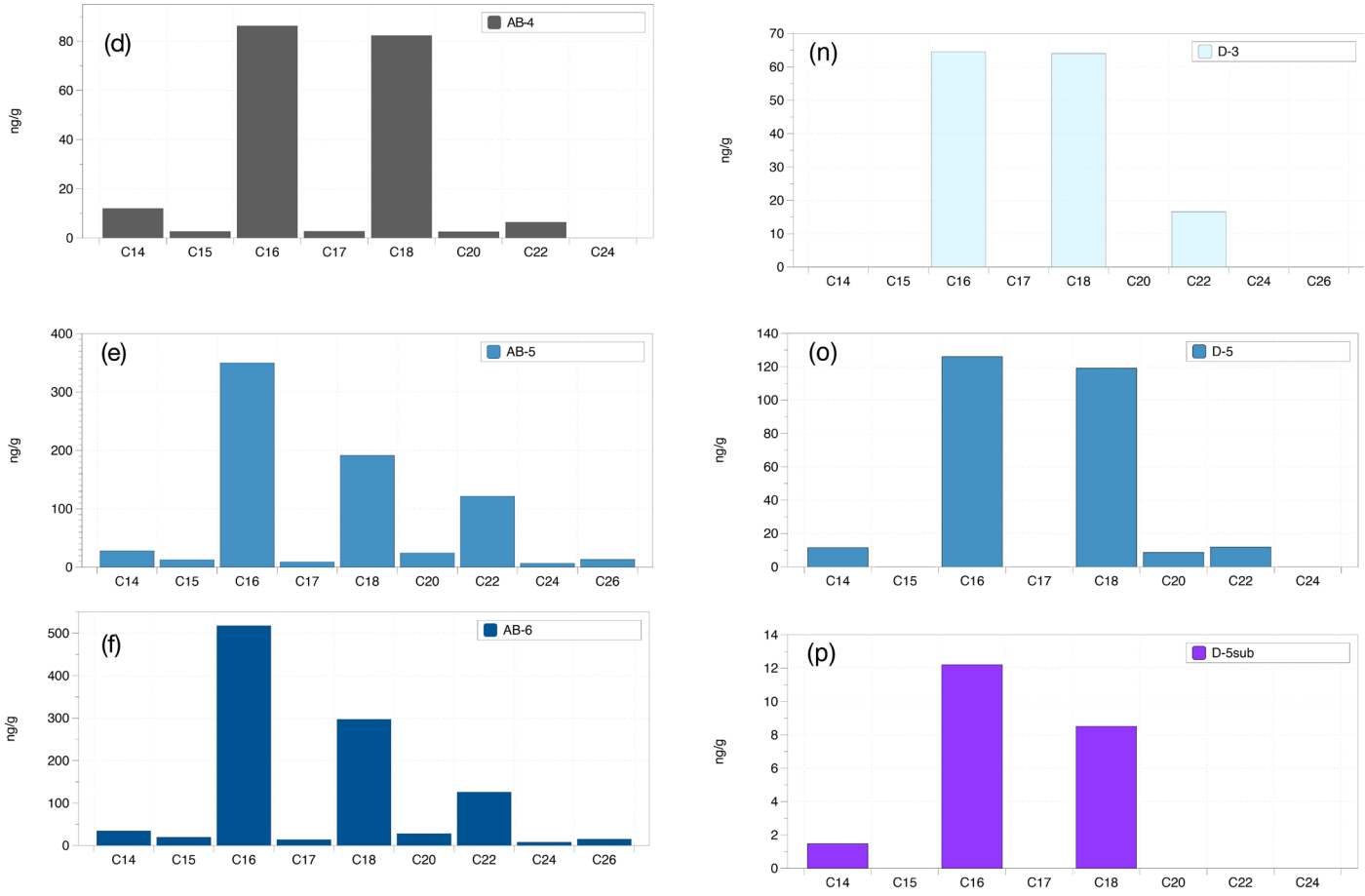

Figure S-2 continued

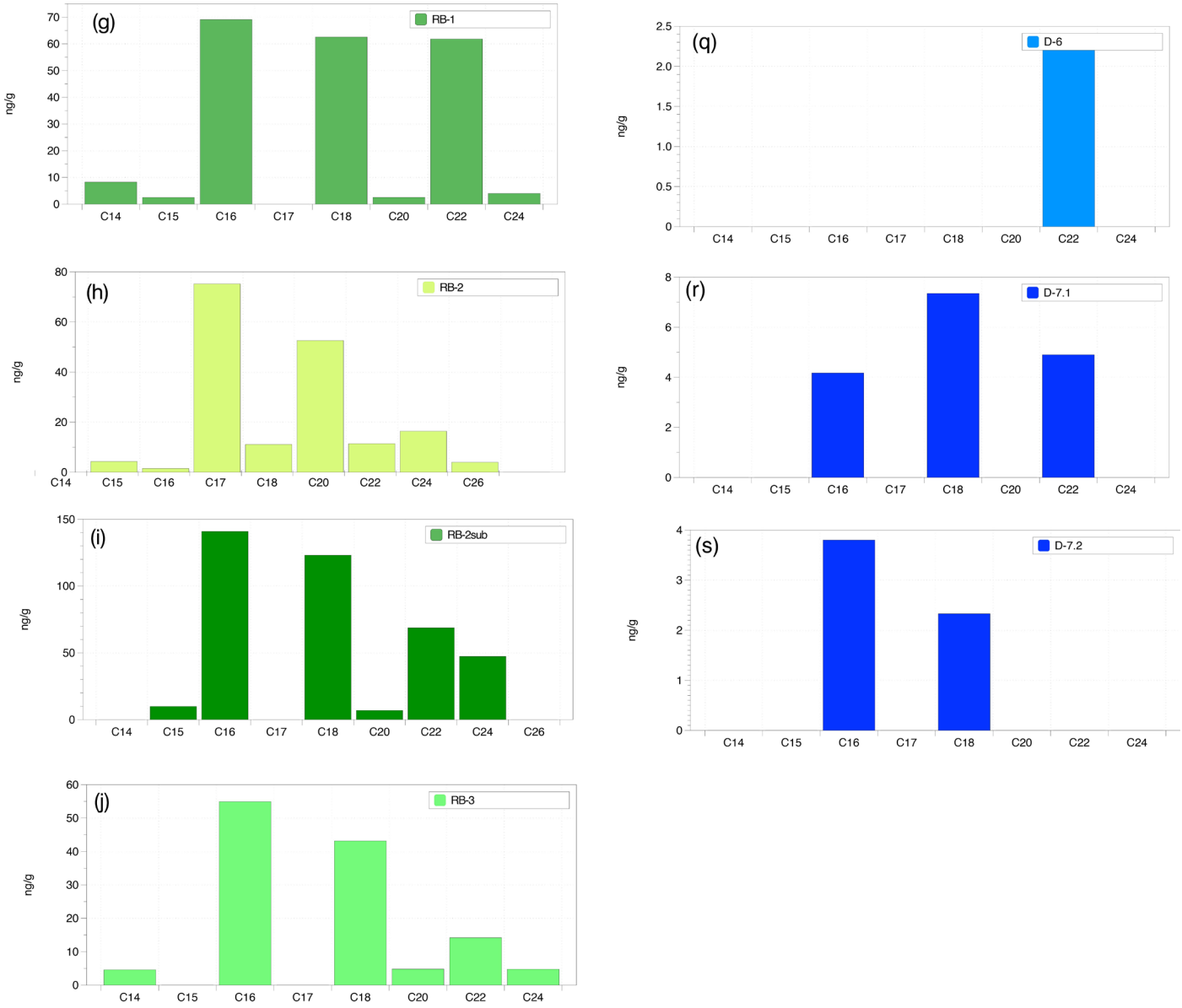

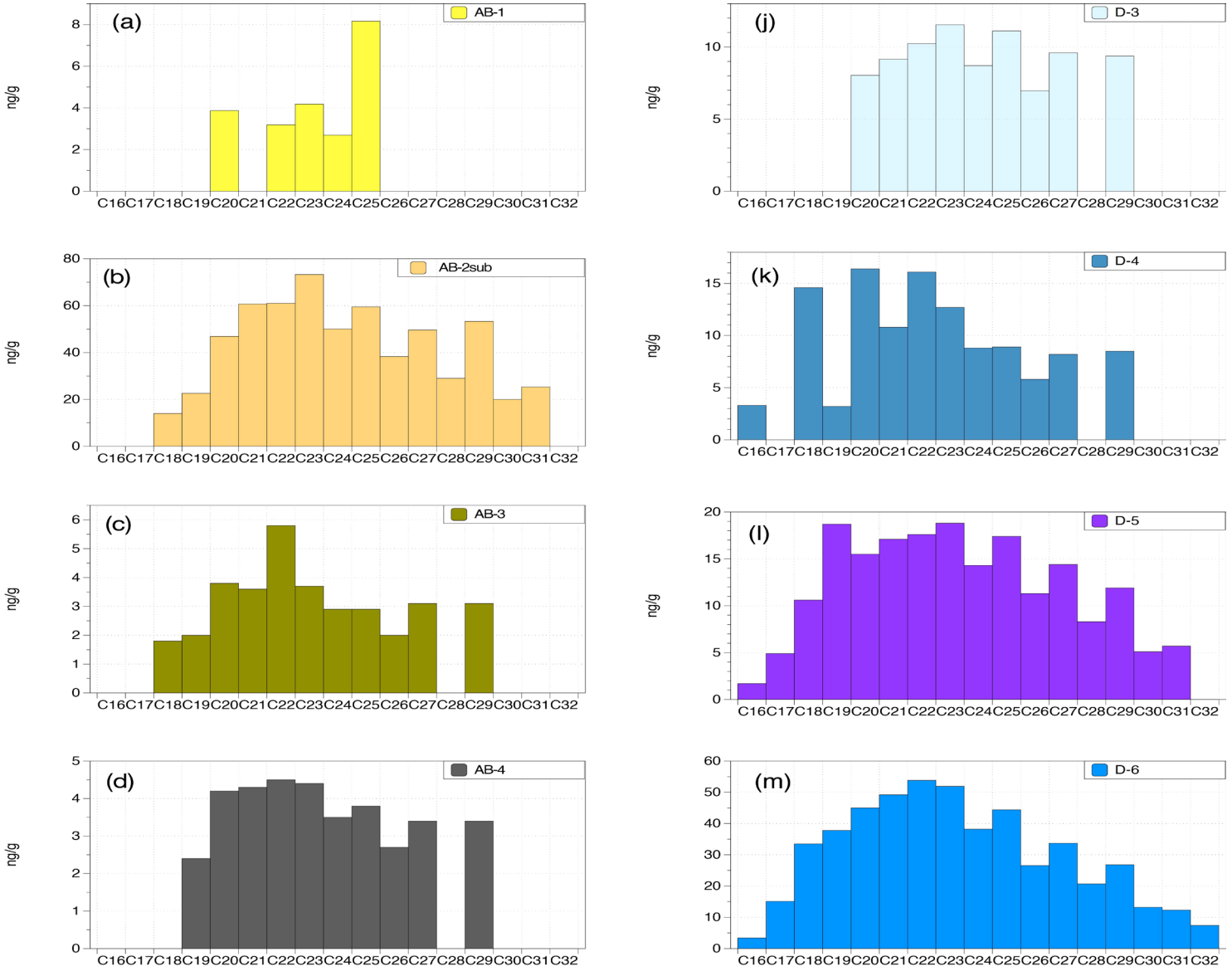

Figure S-3 (across 3 pages) Individual n-alkanes distribution for all samples.

Figure S-3 continued

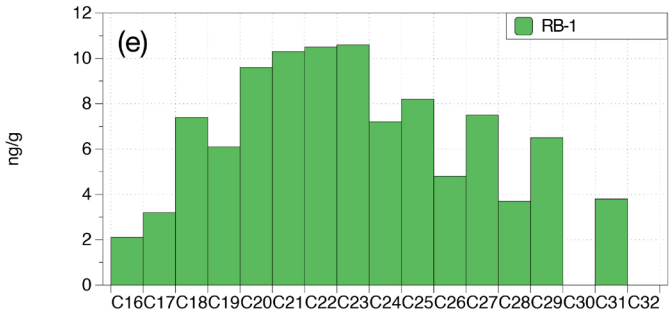

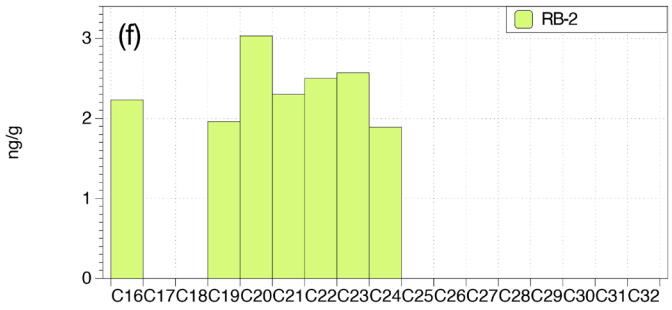

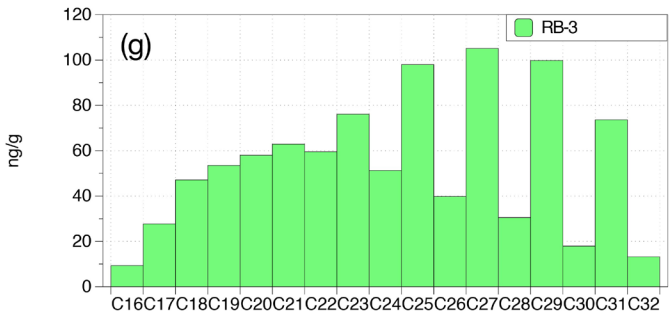

(n)

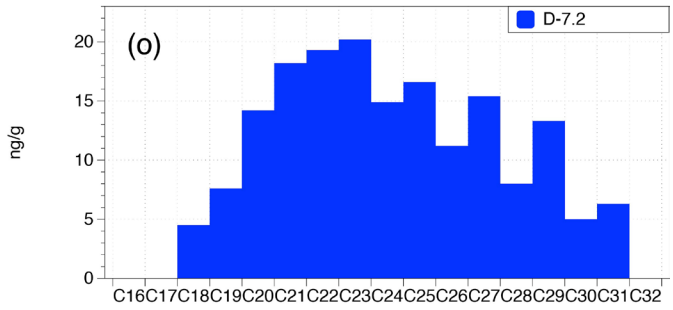

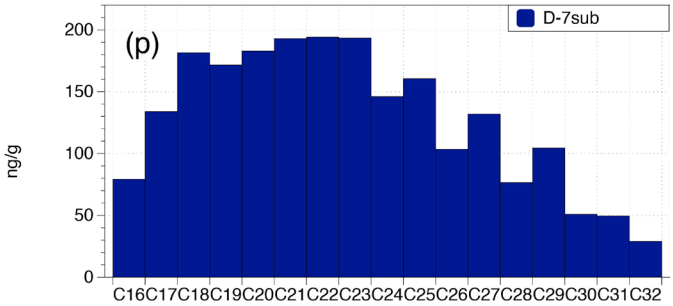

Figure S-3 continued

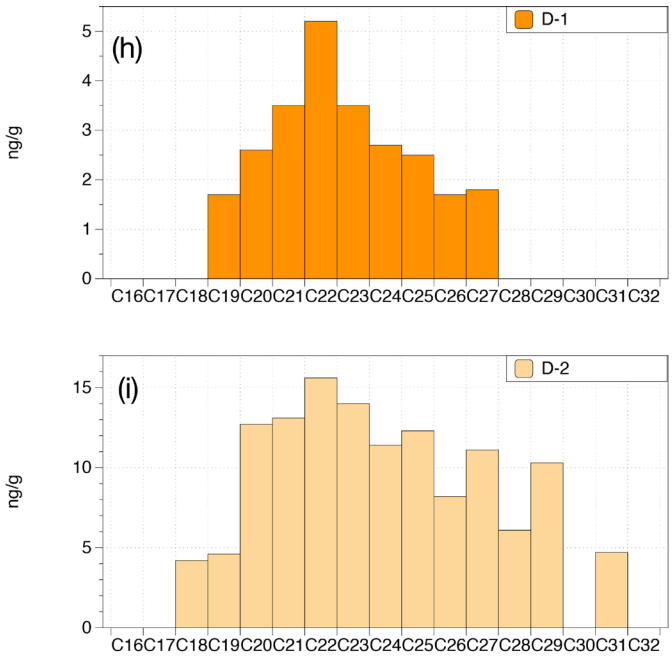

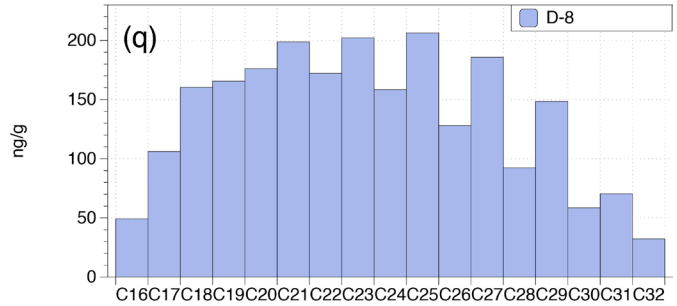

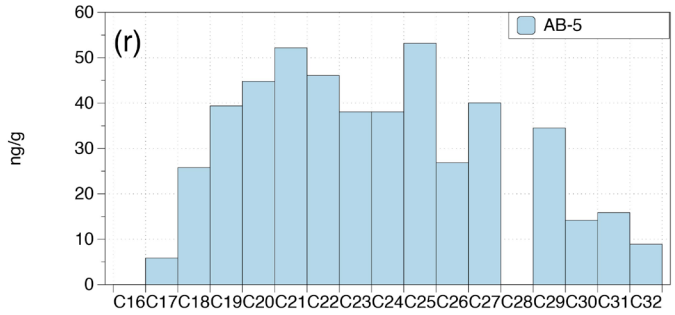

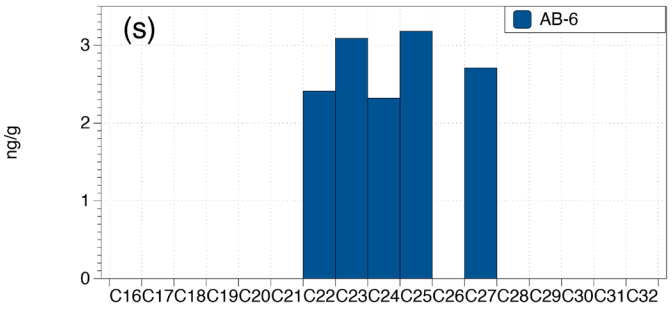

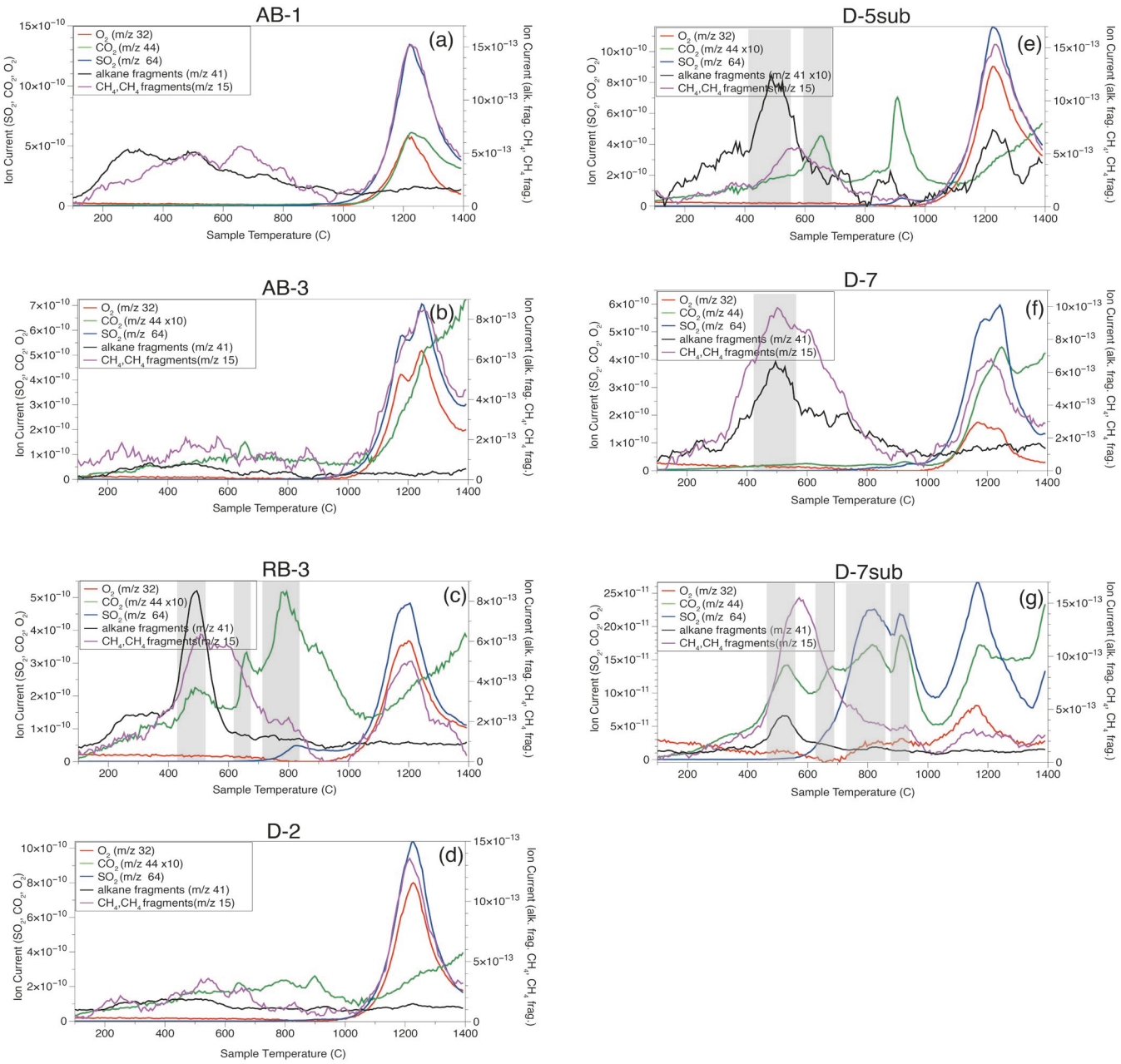

Figure S-4 Evolved Gas Analyses (EGA) results for 7 samples. Active Brine (AB) samples **(a, b),** Relic Brine sample **(c),** Deposit samples **(d, e, f, g).** Grey areas for interesting peaks discussed through main text.

Supplementary Tables

Table S-1 FAMES Normalised to sample mass (ng/g of sample)

Table S-2 n-alkanes normalised to sample mass (ng/g of sample)

Table S-3 Compound specific C isotope results

Tables S-1 to S-3 are available for download (.xlsx) from the online version of this article at http://doi.org/10.7185/geochemlet.2434.

Supplementary Information References

Sánchez-García, L., Aeppli, C., Parro, V., Fernández-Remolar, D., García-Villadangos, M., *et al.* (2018). Molecular biomarkers in the subsurface of the Salar Grande (Atacama, Chile) evaporitic deposits. *Biogeochemistry* 140, 31-52. https://doi.org/10.1007/s10533-018-0477-3

Toney, J.L., Huang, Y., Fritz, S.C., Baker, P.A., Grimm, E., Nyren, P. (2010) Climatic and environmental controls on the occurrence and distributions of long chain alkenones in lakes of the interior United States. *Geochimica Cosmochimica Acta* 74, 1563-1578. https://doi.org/10.1016/j.gca.2009.11.021